Supplementary material for

Multi-Sensor InSAR Assessment of Ground Deformations around Lake Mead and its Relation to Water Level Changes

M. Darvishi[1]*, G. Destouni[1], S. Aminjafari[1] and, F. Jaramillo[1, 2]*

1 Department of Physical Geography, Stockholm University, SE–106 91, Stockholm, Sweden
2 Baltic Sea Centre, Stockholm University, SE–106 91, Stockholm, Sweden
* Correspondence: mehdi.darvishi@natgeo.su.se; fernando.jaramillo@natgeo.su.se

Contents of this file

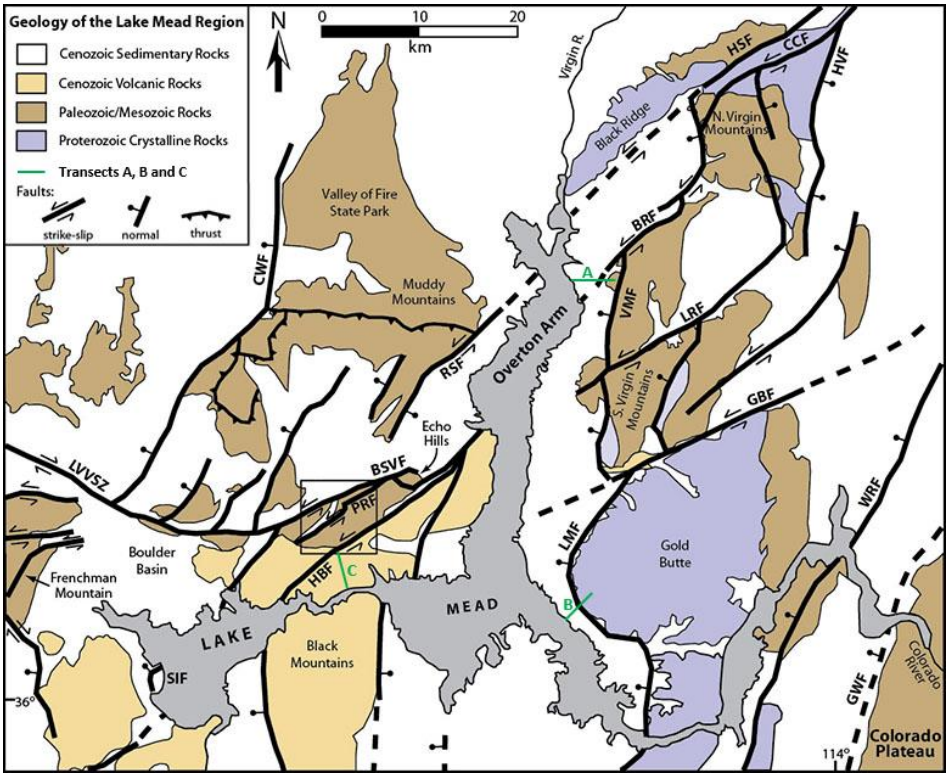

Figure S1. Generalized geology of the Lake Mead region. The acronyms next to the fault lines present the fault names such as Bitter Ridge fault (BRF). The original figure has been taken from [1]. For more information, such as detailed geology, fault, and fold structure of an area nearby the lake (e.g., the Pinto Ridge area indicated by the black square in the figure) please refer to the reference.

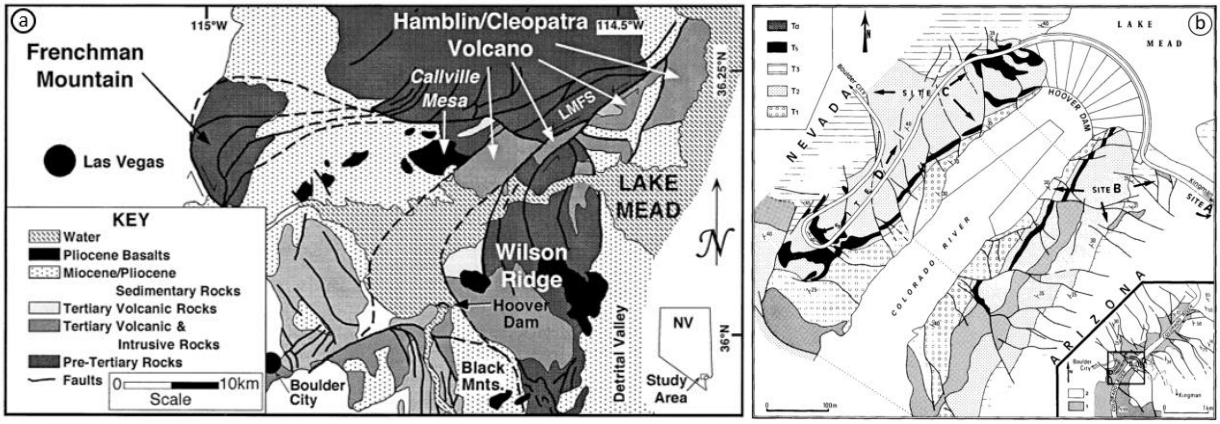

Figure S2. Geological maps of the Hoover Dam and its surrounding. (a) Generalized regional geologic map of the Hoover Dam surrounding, adapted from [2] based on the map from [3]. (b) Geological map of the Hoover Dam locality (after U.S. Bureau of Reclamation, 1950, and written commun., 1981). Faults are shown as thick lines. Dips of layers are in degrees. Tl, conglomerates (dam breccia). T2, lower welded ash-flow tuff (latite flow breccia) with a layer of conglomerate at top (isolated sediments). T3, undifferentiated from bottom to top: upper welded ash-flow tuff (latite flow breccia); volcanic breccia with lenses of sandstone and siltstone (spillway breccia), massive fractured basic latite flow (basic latite). Ts, sill of latite (intrusive latite). Td, dikes of andesite basalt (basalt trachy-dolerite). Lower right corner: highly generalized map of the Hoover Dam area showing selected attitudes in the ash-flow tuff and subjacent lavas and breccias and in undifferentiated lavas and sedimentary rocks above the ash-flow tuff. Intrusive rocks are not shown and faults are shown as thick lines (The source map and related explanations have taken from [3]).

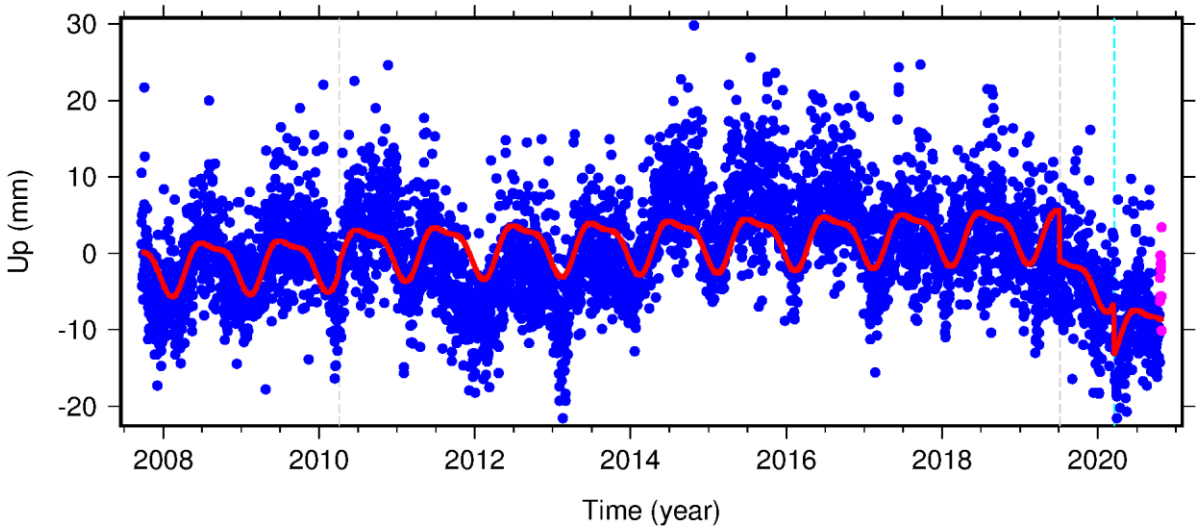

Figure S3. Time-series of the GPS station P006 measurements (vertical component). The time-series plot is provided for 24 hour and 5-minute sample rate solutions. 24 hours site positions using final orbit (blue) and rapid orbit (magenta), which the later one is an estimate of a model fitting the data obtained by the MIDAS algorithm [4]. Times of nearby earthquakes and known equipment change events are marked with grey and cyan vertical dashed lines. The data has been processed and plotted by the NGL on 2020-Oct-15 (source data: http://geodesy.unr.edu/NGLStationPages/stations/P006.sta).

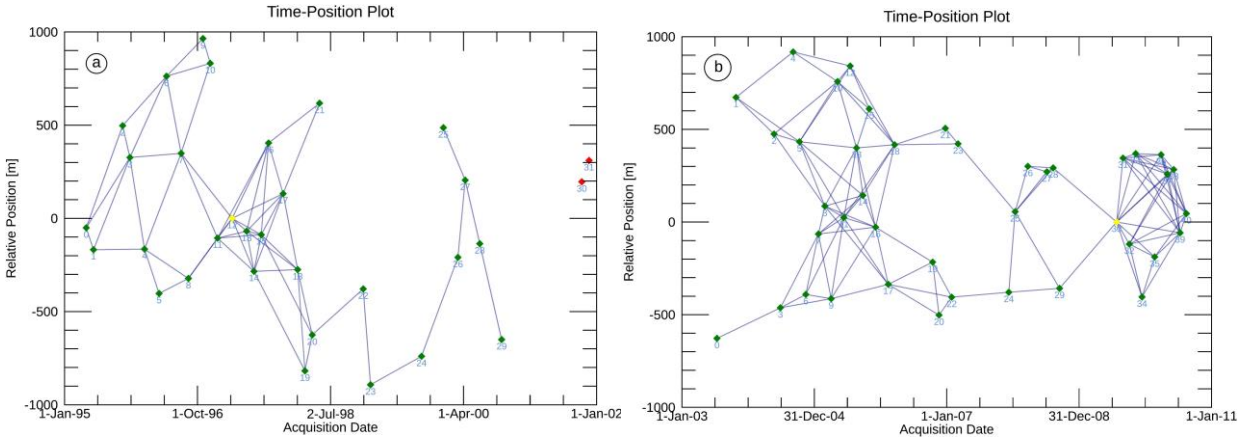

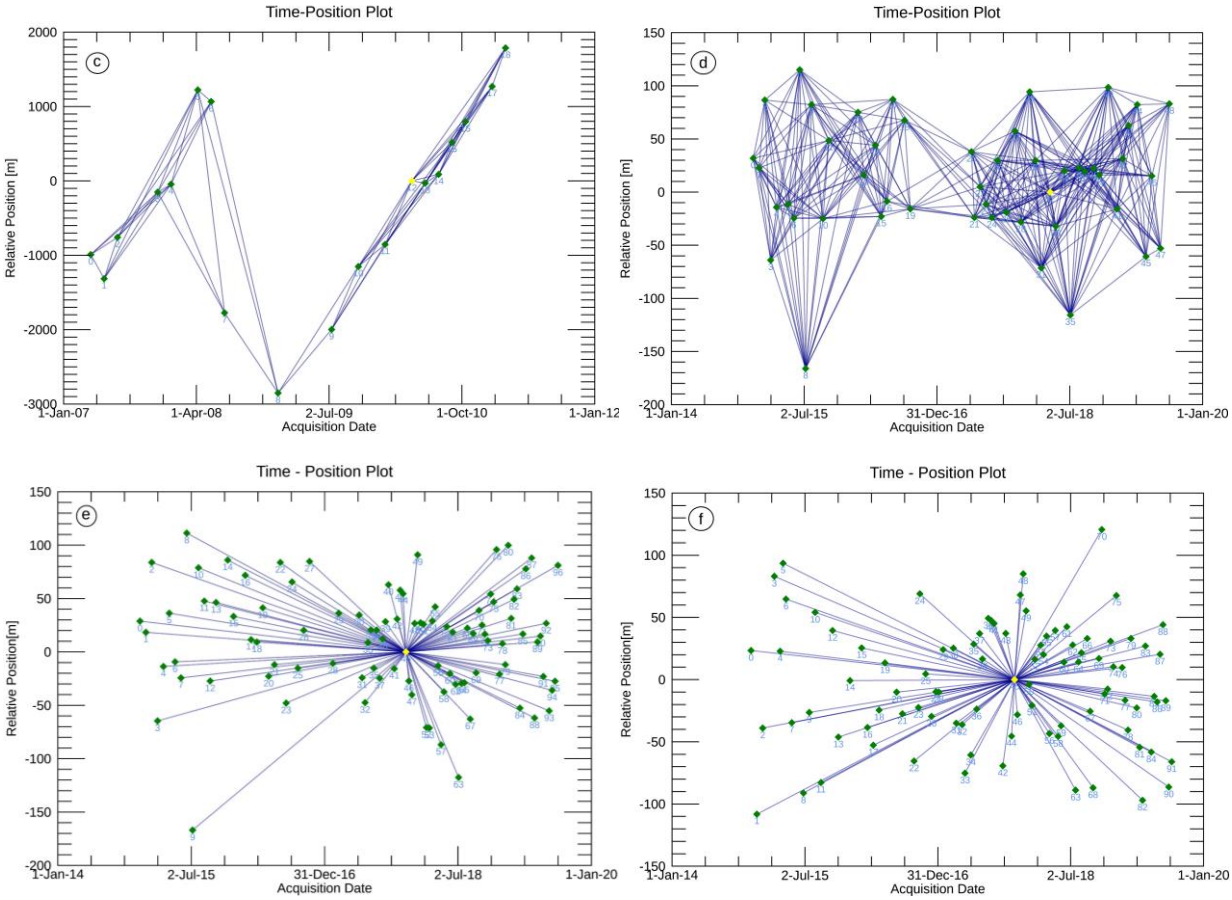

Figure S4. SBAS connection graph of (a) ERS, (b) Envisat, (c) ALOS, (d) S1 (Lake Mead) and PSI connection graph for (e) S1D and (f) S1A related to the Hoover Dam. The relative position (vertical axis) is the distance between the position of the satellite between the different dates (horizontal axis) of the image acquisitions, in relation to their relative position. Each green dot (slave) represents an acquisition from the satellite, and each line the possible interferogram generated from a pair of acquisitions (master and slave). The yellow and red dots indicate the masters and omitted images, respectively.

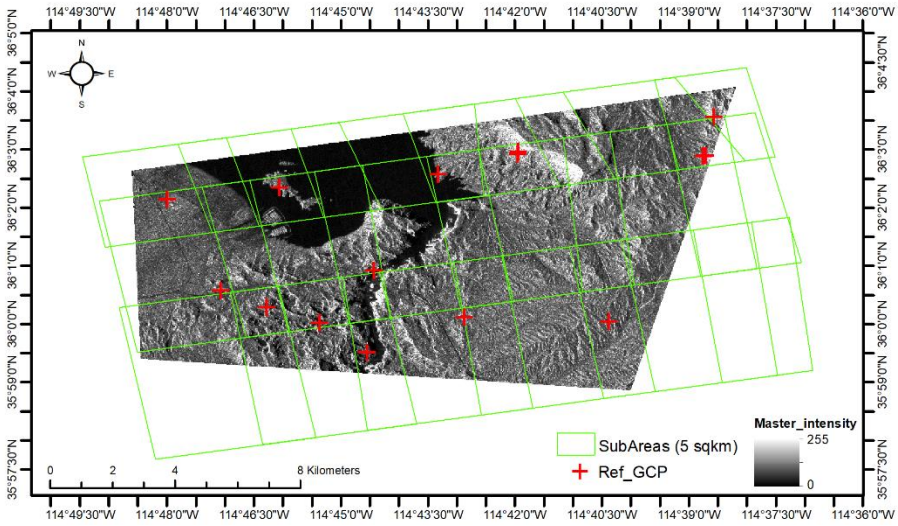

Figure S5. Reference Ground Control point (Ref_GCP) selection in PSI processing. The phase constant removed from all interferograms using several Ref_GCPs that their coherency values are more than 0.99 and its velocities are zero. The searching procedure for the suitable Ref_GCP candidates carried out within the 5 km^2 subareas. The photo in the background is intensity image of S1.

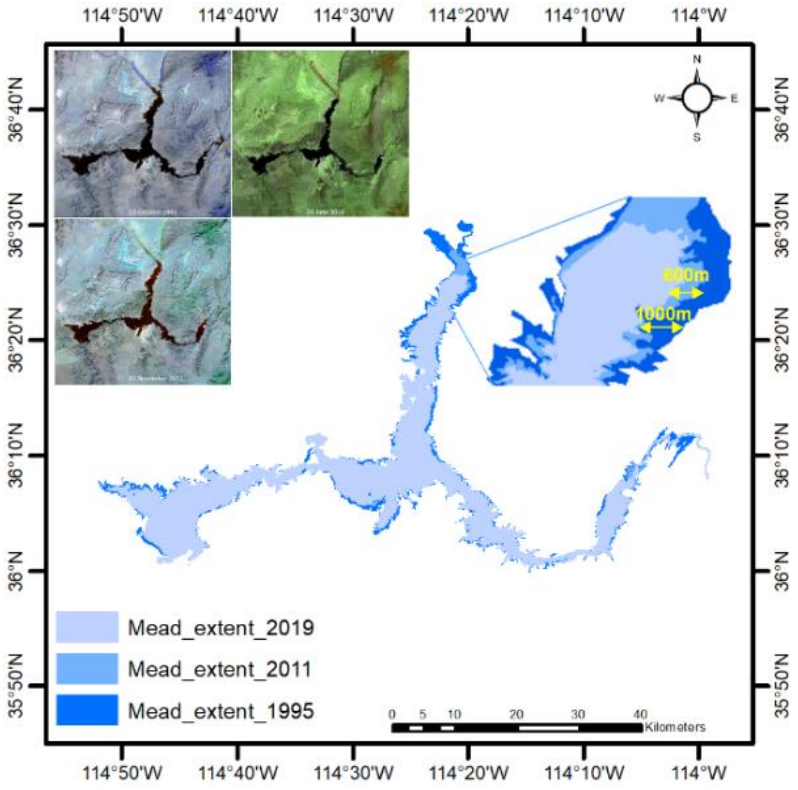

Figure S6. Lake Mead changes in water surface area. Areas extracted by three Landsat images (displayed as three panels on the top-left) taken in 1995, 2011 and 2019; Landsat 5 Thematic Mapper and Landsat 8 Operational Land.

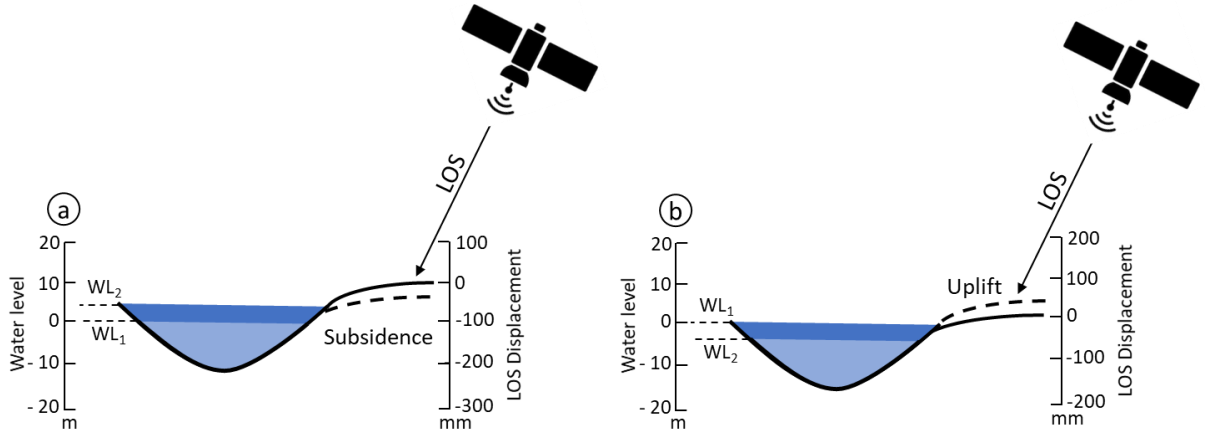

Figure S7. Conceptual model of elastic ground deformation as expected from water load variations. (a) the ground surface has shown by the continuous line at water level one (WL_1). When water level increases to WL_2, the ground subsides due to the additional water load (dashed line). The ground profile gets away from the satellite and the displacement is negative. (b) When water level decreases (from WL_1 to WL_2) the ground rebounds to a higher ground profile (dashed line) and an uplift is observed from the satellite. In this case, the displacement values are positive.

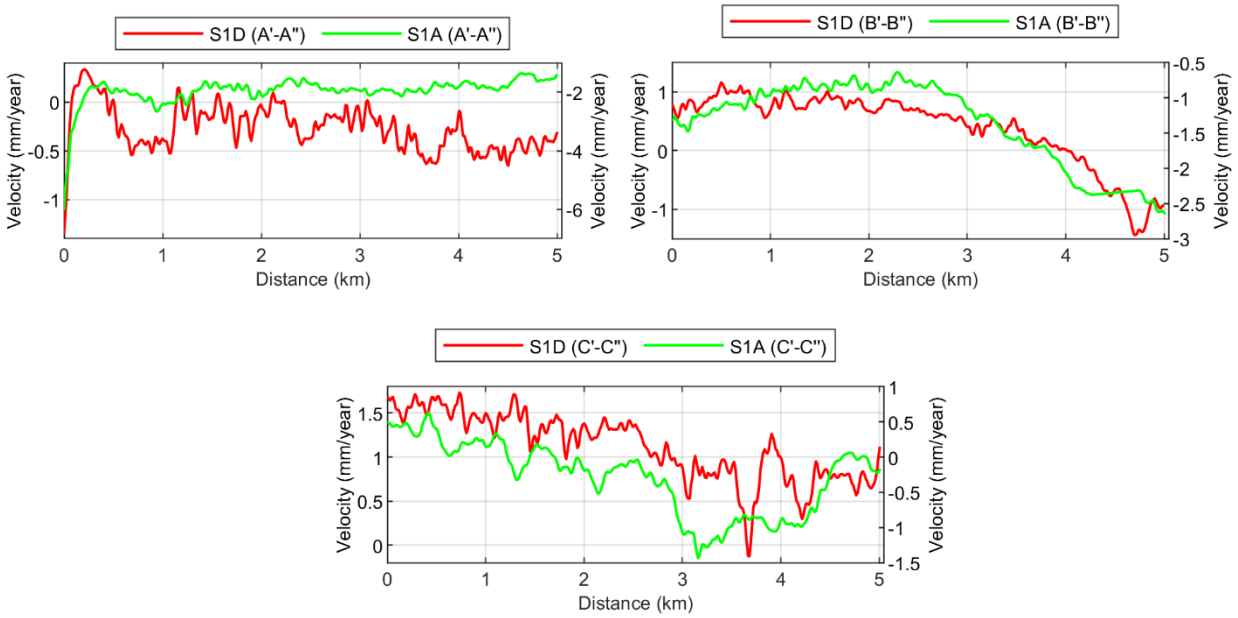

Figure S8. Th cross-comparison of the S1 results in both descnding and ascending modes. The velocity values of the S1 descnding and ascndeing located on the left and right axes respectively.

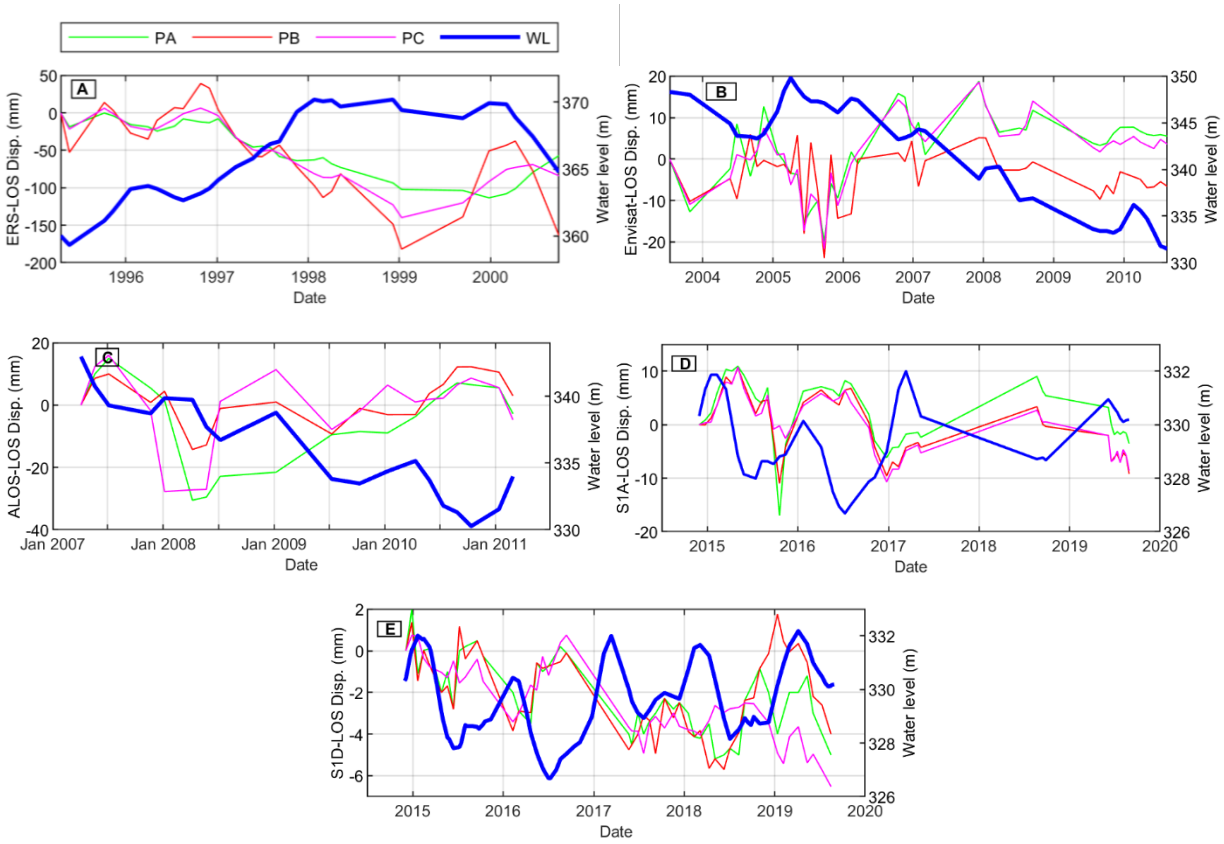

Figure S9. Temporal trends of the water level and ground deformation of a point 500m from the lake along transect A, B and C. Trends for the sensors (a) ERS, (b) Envisat, (c) ALOS, (d) S1A and (e) S1D. Displacement values at 500 m PA: green, PB: red and PC: lila away from the border of the largest water surface area of the lake and corresponding water level (WL; blue).

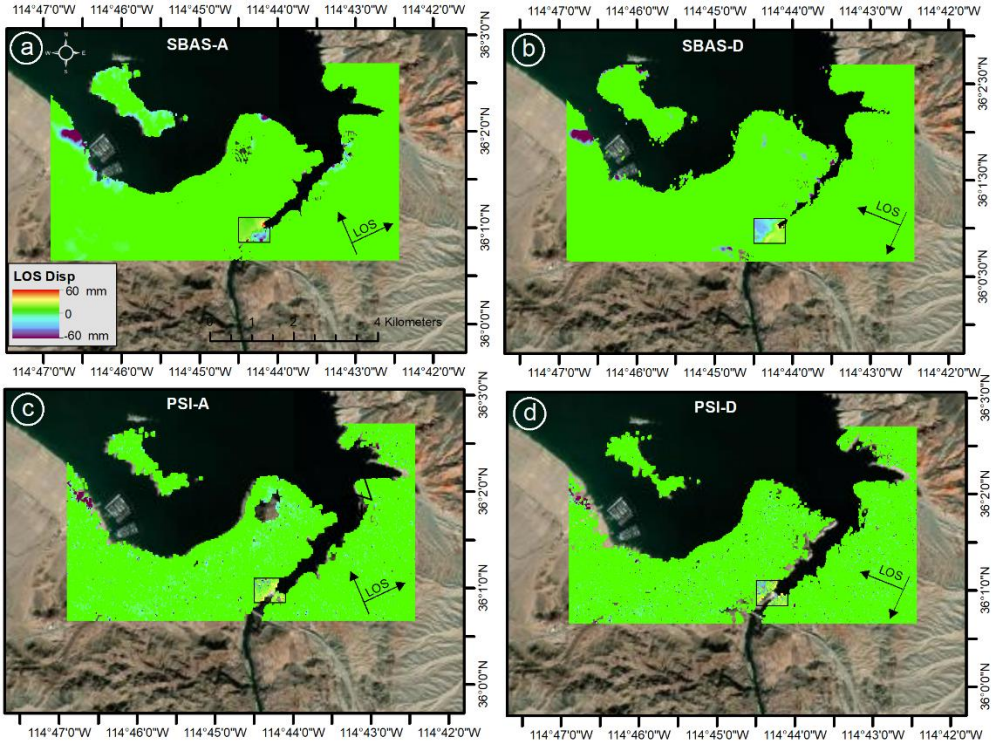

Figure S10. SBAS and PSI processing for the Hoover Dam and its surrounding areas for the S1 period. The deformation maps obtained for both Ascending (A) and Descending (D) modes by SBAS ((a): SBAS-A and (b): SBAS-D) and PSI ((c): PSI-A and (d): PSI-D) techniques. The location of the Hoover Dam has been indicated by the black rectangle on the deformation maps.

References

1. Marshall, S.T.; Kattenhorn, S.A.; Cooke, M.L. Secondary normal faulting in the Lake Mead fault system and implications for regional fault mechanics. *Spec. Pap. Geol. Soc. Am.* **2010**, *463*, 289–310, doi:10.1130/2010.2463(13).

2. Wawrzyniec, T.F.; Geissman, J.W.; Anderson, R.E.; Harlan, S.S.; Faulds, J. Paleomagnetic data bearing on style of Miocene deformation in the Lake Mead area, Southern Nevada. *J. Struct. Geol.* **2001**, *23*, 1255–1279, doi:10.1016/S0191-8141(00)00191-7.

3. Angelier, J.; Colletta, B.; Anderson, R.E. Neogene paleostress changes in the Basin and Range: A case study at Hoover Dam, Nevada-Arizona. *Bull. Geol. Soc. Am.* **1985**, *96*, 347–361.

4. Blewitt, G.; Kreemer, C.; Hammond, W.C.; Gazeaux, J. MIDAS robust trend estimator for accurate GPS station velocities without step detection. *J. Geophys. Res. Solid Earth* **2016**, *121*, 2054–2068.